

MS-DC-UNeXt: An MLP-based Multi-Scale Feature Learning Framework For X-ray Images

Abstract: The advancement of deep learning theory and infrastructure is crucial in the progress of automatic segmentation techniques. Compared with traditional segmentation methods, automatic segmentation methods have considerable strengths such as convenience, accuracy, and so on. However, the drawbacks cannot be neglected. In the laboratory environment, most of the segmentation frameworks are based on deep learning at the cost of sacrificing the lightweight network architecture, adding a lot of parameters in the network to trade for excellent segmentation accuracy. In practical clinical applications, the lack of high computing performance (GPU) machines to maintain operational efficiency poses a huge challenge for the migration from laboratory to clinic. Recently, an alternative to the CNN and Transformer frameworks has been enthusiastically touted, with MLP-based network parameters being significantly decreased as all parameters are learned in the linear layer of the MLP and generate striking outcomes similar to both. Inspired by the MLP-based framework, we recommend leveraging the MS-DC-UNeXt as an alternative solution for medical image segmentation, which is mainly composed of Tokenized MLP block, Dual Channel block(DC-block), and Bottleneck (Res-ASPP). Among them, Tokenized MLP block has played a crucial role. On the one hand, adding DC-block and Res-ASPP block in a U-shape network can obtain Multi-Scale features. On the other hand, choosing two linear layers can acquire the self-attention mechanism similar to Transformer, which enables the MS-DC-UNeXt model to obtain local-to-global semantic dependency, and dramatically increase the operational efficiency of the model. We perform extensive validation on a benchmark dataset (ISIC 2018) and conduct medical image segmentation on the other two experimental datasets of X-rays Images. The experimental results show that MS-DC-UNeXt can achieve a better segmentation result on X-rays images than the U-shape model of state-of-the-art and successfully achieves the goal of Accuracy-speed trade-off.

Keywords: MLP-based; Multi-Scale feature learning; laboratory to clinic; Depthwise Separable Convolution; X-ray

1 Introduction

With the improvement of deep learning theory and hardware facilities, computer vision has achieved a spectacular breakthrough in the fields of medical organ segmentation, disease detection, and cell classification. Standard medical diagnostic scans (mainly including X-ray, CT (Computed Tomography), MRI (Nuclear Magnetic Resonance Imaging), dermoscopy, and other modalities) play an essential role in the diagnosis and evaluation of diseases. In hospitals, specialists, including doctors and physicians from multi-disciplinary departments such as imaging, pathology, and endoscopy, jointly interpret the pathological images of patients. As there are a lot of noise points in the medical image, which dramatically enhances the difficulty of extracting the critical information, and how segment the medical image correctly and speedily is a tricky issue for medical image segmentation to help doctors identify the patient's lesion quickly.

As a simple and cost-effective way to detect disease, X-ray is frequently applied to detect skeletal lesions, exceptionally soft tissue lesions. X-ray imaging is prone to small amounts of Artifacts due to clothing, soft tissue thickness, and the angle at which the patient is standing. Meanwhile, some X-ray images of finger bones do not have clear borders, which increases the difficulty of separating the background image and the divided object.

It is well known that precise and fast medical image segmentation can assist doctors in diagnosing diseases and making appropriate treatment strategies for patients. Manual or semi-automatic segmentation (traditional) is better than automatic segmentation (based on deep learning) in the accuracy of a small margin, but there are obvious limitations. It takes a lot of time and resources to manually identify and mark the patient organ boundary by many experienced doctors and experts, and the final marking result is entirely subjective. In front of a highly challenging medical image, although combining multi-disciplinary departments can strengthen the accuracy of the diagnosis, it is still impossible to ensure the correct segmentation and requires more resources than before.

Compared with traditional segmentation methods, automatic segmentation methods have the advantages of convenience and accuracy of prediction and so on [1], but the existing drawback can not be neglected. In the laboratory environment, most networks based on deep learning have significant parameters and high computational complexity in trade for accurate segmentation boundaries. However, in practical clinical applications, the lack of high computing performance (GPU) machines to maintain their operational efficiency poses an enormous amount of challenges for the migration from laboratory to clinic.

Currently, the mainstream automatic segmentation methods rely on a symmetric Encoder-Decoder U-shaped framework. Motivated from FCN (Fully Convolutional Networks), the encoder of UNet networks [2-3] uses a module combining convolutional layers and downsampling to extract features by increasing the depth of the receptive field layer by layer. The high-resolution and low-resolution features are linked together by skip connections in the decoder, which compensates for the

missing pixel values in downsampling to obtain accurate location information. In recent years, UNet and its extension methods have become a de-facto choice for medical image segmentation. Since the capability of extracting local features, FCNN-based models perform well in medical image segmentation tasks. Many important improvement frameworks have appeared on the foundation of FCNN, such as UNet [3], UNet++ [4], UNet3+ [5], Attention-UNet [6], ResU-Net++ [7], DC-UNet [8], and so on. Recently, Transformer-based architecture has achieved a state-of-the-art effect across multiple medical image challenge datasets with the local-to-global attention mechanism. Stimulated by the great success of transformer in NLP (Natural Language Processing), Dosovitskiy et al.[9] proposed ViT (Vision Transformer) and applied it to the field of computer vision, and it has been fully demonstrated on image classification tasks. To improve the generalization capability of ViT, based on it, Liu et al.[10] improved the MSA (Multi-headed Self-attention) module and replaced it with the SW-MSA (Shifted Windows Multi-Head Self Attention) module, which combines multiple Swin-Transformer blocks into a Swin-Transformer. The ability of target detection and semantic segmentation has been improved by restricting messages to communicate between adjacent windows. Transformer-based U-shape architecture, including TransUNet [11], Swin-UNet [12], SUNet [13], and so on, have been fully applied to medical image segmentation tasks.

Subject to the practical clinical environment, we propose simplifying the mainstream automatic segmentation frameworks to build lightweight segmentation networks to augment the generalization ability of the models on various segmentation tasks. Recently, an alternative scheme distinct from the CNN and Transformer frameworks has been touted, where all parameters are learned from the linear layer of the MLP, yielding surprising results that resemble both, and more research is underway [14-15]. Inspired by the MLP-based model, we recommend leveraging the function of Tokenized MLP block in the framework of MS-DC-UNeXt for 2D medical image segmentation, which is mainly composed of Tokenized MLP block, DC-block, Bottleneck(Res-ASPP). Note that all the improvements we have made are still based on UNet. We replace the single-layer convolution module in UNeXt [16] with the DC-block [8] to obtain Multi-Scale features. Meanwhile, an Attention Gate is added to the DC-block in the decoder to enhance the segmentation performance by suppressing the skip connections of unrelated regions. In Bottleneck, we use Dilated Convolution with ResNet (Residual Network) to expand the receptive field to get Multi-Scale contextual information and to solve the gradient disappearance and gradient explosion problems. To help the model learn more essential features, we use axial shifts (a shifted windows module similar to Swin-Transformer) to project convolutional features. More local features can be acquired while prioritizing the image's global attributes. Due to the adoption of two linear layers to replace self-attention, the replacement of Standard Convolution with Depthwise Separable Convolution, and the use of ResNet in Bottleneck, compared with the FCNN-based and Transformer-based segmentation frameworks, the model can significantly minimize the parameters and operational complexity, thus achieving the goal of accuracy-speed trade-off. We evaluate the MS-DC-UNeXt model thoroughly on the

ISIC 2018, BAA, and COVID-19 CXR dataset. We find that MS-DC-UNeXt has an incomparable and massive advantage over the mainstream segmentation models. Note that compared with UNeXt, MS-DC-UNeXt only increases the Params Size by 2.29 MB, and the model predicts performance benefit (MIoU) from 0.61% to 1.65% on the three datasets.

Concretely, our contribution can be summarized in four major fields:

1. Based on the tokenized MLP block, we have designed a symmetric Encoder-Decoder MS-DC-UNeXt model, leveraging DC-block and Res-ASPP block to obtain Multi-Scale features.

2. Two linear layers are used to get a self-attention mechanism similar to the transformer, which makes the MS-DC-UNeXt model get semantic dependency of local-to-global.

3. We have improved and enlarged the scope of use of the original UNeXt model, and the segmentation effect is significantly enhanced with a slight amount of additional parameters and operational complexity.

4. Our proposed MS-DC-UNeXt model has extensive validation on a benchmark dataset (ISIC 2018) and performs medical image segmentation on two experimental datasets of X-rays Images, from which we can see that the model has the best ability to generalize and migrate on X-rays Images.

2 Related Works

2.1 Medical Image Segmentation

Early medical image segmentation mainly relies on edge detection, threshold segmentation, machine learning, and other methods. However, the medical image has existed some troubles, such as blurred boundaries, dense noise points, low contrast, and significant variation of organ shape in different periods. It is tough to directly leverage traditional methods for medical image segmentation [17-18]. With the breakthrough made by CNN in handwritten font recognition, the method of deep learning has gained popularity in the field of image processing [19]. Jonathan et al.[2] proposed the first Convolutional neural network FCN (Fully Convolutional Networks), which laid the foundation for semantic segmentation. FCN uses a fully convolutional neural network to produce input images of all sizes, and the final output is the exact pixel-level prediction of the original image. The receptive field of FCN is too small to be analyzed with global semantic information, based on FCN, Ronneberger et al.[3] used an improved Encoder-Decoder structure UNet with skip connections for accurate segmentation of medical images. Since UNet tends to lose many low-level features during up-sampling, Oktay et al.[6] proposed a network Attention-UNet with an Attention Gate to suppress the skip connections of low-correlation regions for better segmentation. Motivated by the attention mechanism, Trebing et al.[20] applied a channel and spatial attention mechanism (CBAM) to the input image. Compared with the original Attention-UNet, SmaAt-UNet has realized more accurate predictions with significantly reduced parameters and computational complexity. Xu et al.[21] used a deeper and more compact split attention structure, DCSAU-Net, to access valuable features in medical images by continuously increasing the depth of convolution and

combining split attention. Due to the lack of long-distance dependence on a range of FCNN-based networks, Chen et al.[11] proposed a new segmentation framework, TransUNet, with a global self-attention mechanism, in which the ViT (Vision Transformer) module is added to the encoder to obtain accurate spatial location information. Inspired by the Swin Transformer, Cao et al.[12] submitted a kind of U-shape pure Transformer-based network Swin-UNet. Set up a symmetric encoder-decoder network based on the Swin Transformer block, and enter each token into the decoder to learn the feature representation. Experimental results show that Swin-UNet has good robustness and segmentation precision on multiple medical image segmentation datasets. Compared with the CNN-based model, the Transformer-based model is prone to many parameters, higher computational complexity, and more incredible pre-trained difficulty, which is challenging to implement despite the pre-trained strategy.

2.2 MLP-based methods

Tolstikhin et al.[14] proposed the MLP-Mixer framework, which can be used as an alternative to Transformer and CNN, discarding the traditional convolution and attention modules. The MLP-Mixer adopts two types of MLP layers: channel mixing MLP and token mixing MLP. Each row and column are used as input, respectively. Two kinds of MLP layers are executed alternately to exchange information on two different dimensions. The proposed MLP Mixer framework achieves a segmentation effect similar to ViT on JFT-300M and ImageNet datasets. Because the MLP Mixer framework does not have good generalization ability, extending it to downstream tasks is difficult. At the same time, MLP Mixer seldom uses low-level semantic information. In actual image segmentation, not all pixels need long-distance dependency to obtain global semantics. Based on the initial MLP Mixer framework, Lian et al.[15] submitted an AS-MLP framework with axial shifts to focus on local information. AS-MLP adds a shift window to the MLP Mixer, extracts features from the vertical and horizontal dimensions, and then combines features from the two dimensions to achieve information exchange and fusion. Axial shifts were similar to AS-MLP, Valanarasu et al.[16] have incorporated tokenized MLP blocks into UNet and established the UNeXt framework with a symmetric Encoder-Decoder. The framework extracts local-to-global semantic information corresponding with different axial shifts by sequentially carrying out feature transformations on Width and Height dimensions for the input feature maps (not a simple summation of features in two dimensions like AS-MLP). This MLP-based UNeXt framework can significantly shrink the model parameters and time complexity and is ideally validated on ISIC 2018 and BUSI datasets.

3 Methods

3.1 Network Design

MS-DC-UNeXt is a symmetric MLP-based U-shape network consisting of four Tokenized MLP blocks, four DC-blocks, and a Bottleneck (Res-ASPP). In the encoder, we replace the traditional convolutional (single layer) module with DC-blocks for the purpose of learning more features to improve the segmentation precision. Furthermore, the Tokenized MLP block projects the features into tokens and uses axial shifts to transform the features in Width and Height dimensions in turn. The tokens are transformed by using axial shifts to obtain more position information. In the decoder, upsampling is used to re-create medical images. It compensates for the loss of local features during the encoder by combining low-resolution features in an encoder and high-resolution features in a decoder by using a skip connections. Note that in the decoder, in addition to using Tokenized MLP block to capture the semantic information from local to global, we also introduce the Attention Gate mechanism before the DC-block to suppress skip connections in non-related regions, which contributes to retaining more high-level semantic information to get more refined segmentation. Note that the comparison experiments were performed under the same conditions as possible, and in each layer, we kept filters the same as UNeXt. On this basis, we also propose a more lightweight MS-DC-UNeXt-S framework to complement the MS-DC-UNeXt model, which is well-validated on three datasets.

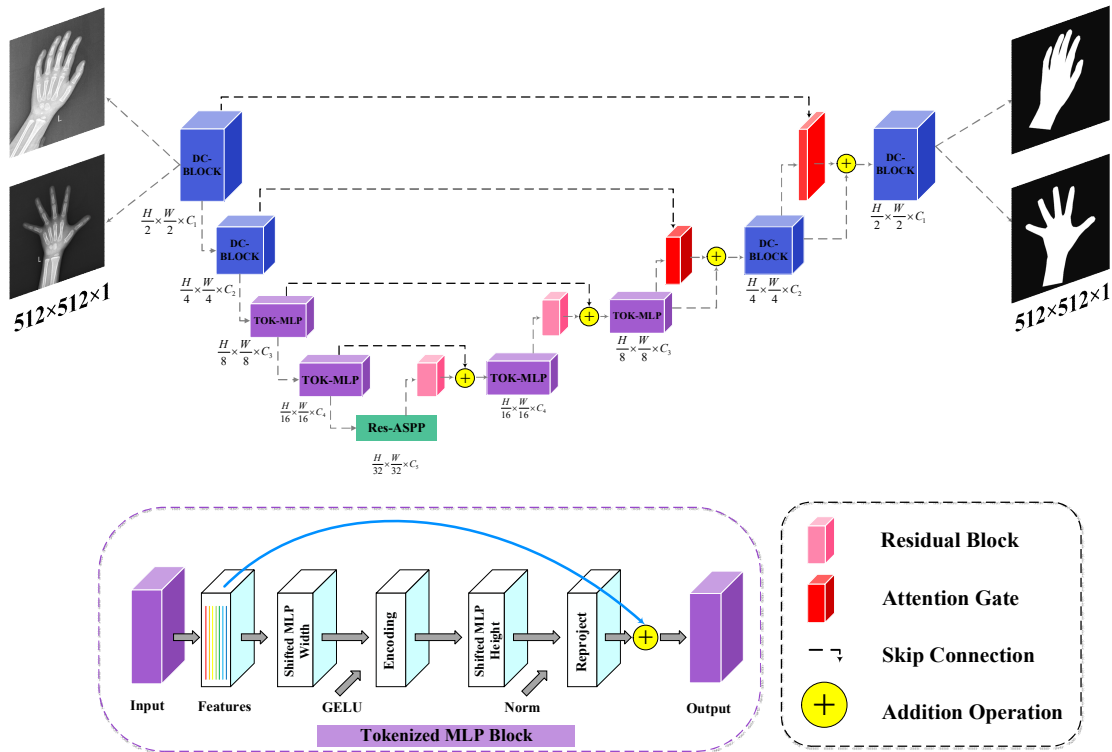


Fig.1. The architecture of MS-DC-UNeXt

3.2 DC-block with Attention Gate

Aiming at the problem of fuzzy objects and background interference in finger bones and pneumonia images, we present DC-block with an Attention Gate structure to obtain more proportion of Multi-Scale features, so as to correctly separate background pictures from objects that need to be split. The Attention Gate can suppress the skip connections in non-related regions, thereby improving the accuracy of the segmented objects. As shown in Fig 2, the Attention Gate contains two parts of the input, one is the semantic information from the decoder below, and the other one passes the semantic information from the encoder to the decoder through the skip connections and the final result is the input of DC-block. In order to obtain more semantic features, we have adopted a two-channel sequence of 3×3 convolutional layers to replace the single-layer convolution and combine the semantic features of the convolution layer of dual channels to get the output. Note that the number of three 3×3 filters is $W/6$, $W/3$, and $W/2$, respectively, and W is the number of filters in each layer. In order to minimize the hazard caused by overfitting, we perform batch normalization operation after the Activation Function (RELU) of each layer, and the final output is activated by the Sigmoid function.

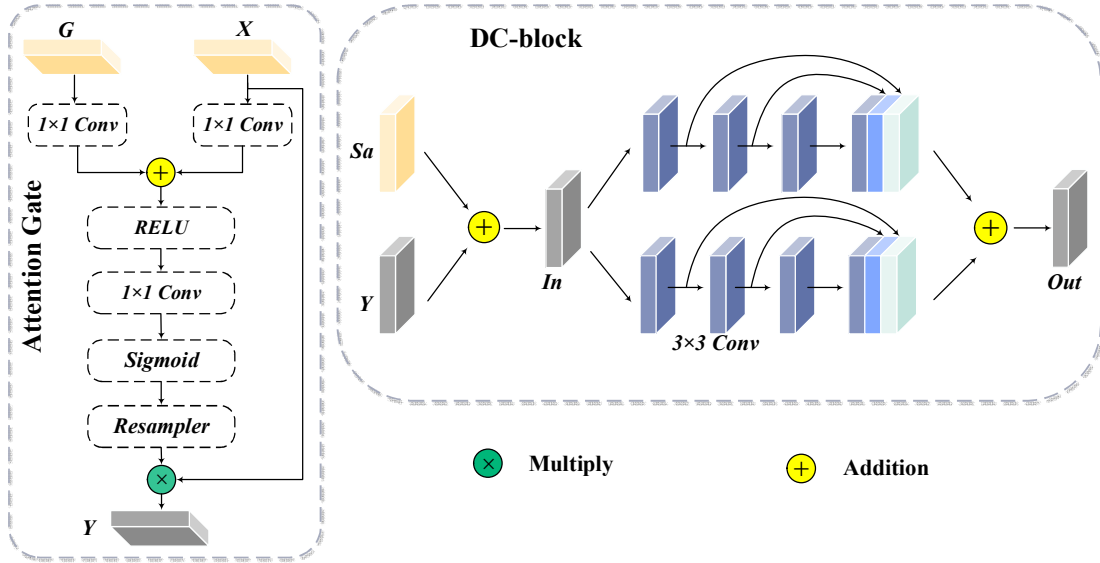


Fig.2. We proposed DC-block and Attention Gate architecture in the decoder

3.3 Tokenized MLP block

To improve the performance of the model while simultaneously reducing the number of parameters and computational complexity, Tolstikhin et al.[14] first proposed a structure MLP-Mixer that is different from transformer-based structure, which can gain global dependency similar to self-attention by using linear layers, and it has achieved better results in several datasets. Lian et al. [15] introduced the AS-MLP structure with axial shifts based on the MLP-Mixer, which was the first application of the MLP structure to the downstream tasks. Since MLP-Mixer utilizes more global dependencies, not all pixel points are required to use long-range dependencies in practical tasks, which will lead to a large number of missing low-

level features. In response to the limitations of MLP-Mixer, AS-MLP adds a window to MLP-Mixer, as shown in Fig 3(b). In axial shift, all features are first projected onto a linear layer through channel projection. Then shift the features in both the vertical and horizontal dimensions simultaneously, and reunite together the features in both two dimensions. Finally, project the features that have been merged. AS-MLP merged the two dimensions to realize the flow of information in different spatial positions to attain the semantic dependency from local to global. Motivated by a series of MLP-based models, Valanarasu et al.[16] proposed the UNeXt framework, which successfully integrated the axial shift mechanism with UNet, and the model has yielded significant benefits on ISIC 2018 and BUSI datasets.

The specific architecture of the Tokenized MLP block is illustrated in Fig 3(c), where we start by projecting all the features into the token (similar to AS-MLP), and then we utilize the axial shift mechanism to project the features in the width and height directions(there is an order of dimension projection, and the token is first shifted in the width direction. Not the same as AS-MLP, projecting both directions simultaneously), respectively. The shift operation is contribute to making the MLP only focus on regions of higher correlation and suppress learning features of regions of lower correlation, which enables it to learn more low-level semantics. A Tokenized MLP block comprises two MLP blocks, taking width direction as an example and similarly in the Height direction. By dividing the features into h different partitions, we first shifted the features in the width direction by j positions. Then we use Depthwise Separable Convolution to transfer the features in the width direction. Eventually, GELU is employed to implement the feature extraction process, which can preserve the previous useful features while abandoning the features with a low degree of correlation to the task. To alleviate the hazard from over-fitting, following this module, we add a layer normalization for normalization operation. After feature extraction, we transfer the features in the width direction to the height direction.

The formula for performing axial shift operations in each of the two directions is given below:

$$X_{shift} = Shift_W(X); T_W = Tokenize(X_{shift}) \quad (1)$$

$$Y = f(DWConv((MLP(T_W)))) \quad (2)$$

$$Y_{shift} = Shift_H(Y); T_H = Tokenize(Y_{shift}) \quad (3)$$

$$Y = f(LN(T + MLP(GELU(T_H)))) \quad (4)$$

where T represents tokens, W represents width, H represents height, $DWConv$ represents Depthwise Separable Convolution, and LN represents layer normalization. To control the same experimental conditions, we do not change the size of the embedding dimension H , which remains at 768.

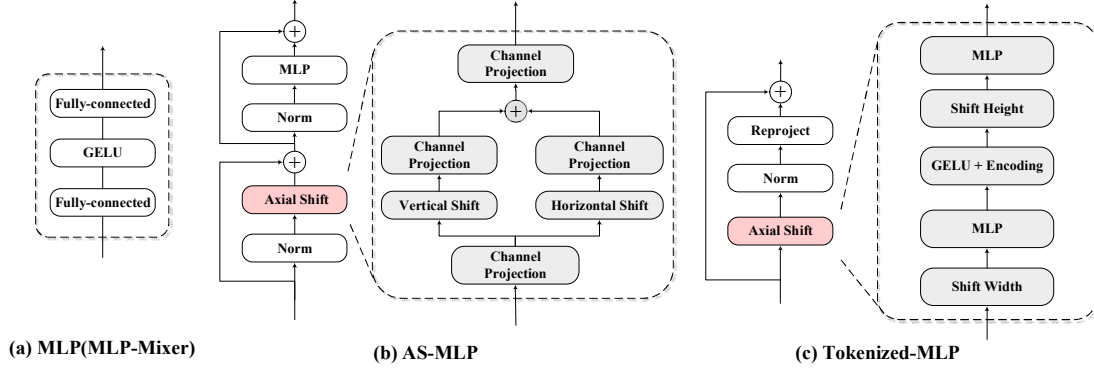


Fig.3. Compare the structures of two Axial Shifts

3.4 Bottleneck

The proposed Bottleneck (Res-ASPP) serves as a bridge to connect the encoder and decoder, and we make the receptive field learn the Multi-Scale feature representation by setting the dilation rate to 4, 8, 16, and 24, respectively. ASPP mainly includes the traditional convolutional layer, the Batch Normalization(BN), and the Activation function (RELU). Since ResNet can decrease the number of parameters in the network while restricting the depth of the receptive field, and solving the issues of gradient disappearance and gradient explosion, we utilize ResNet to replace the traditional convolutional layer. The framework of Res-ASPP is shown in Fig 4.

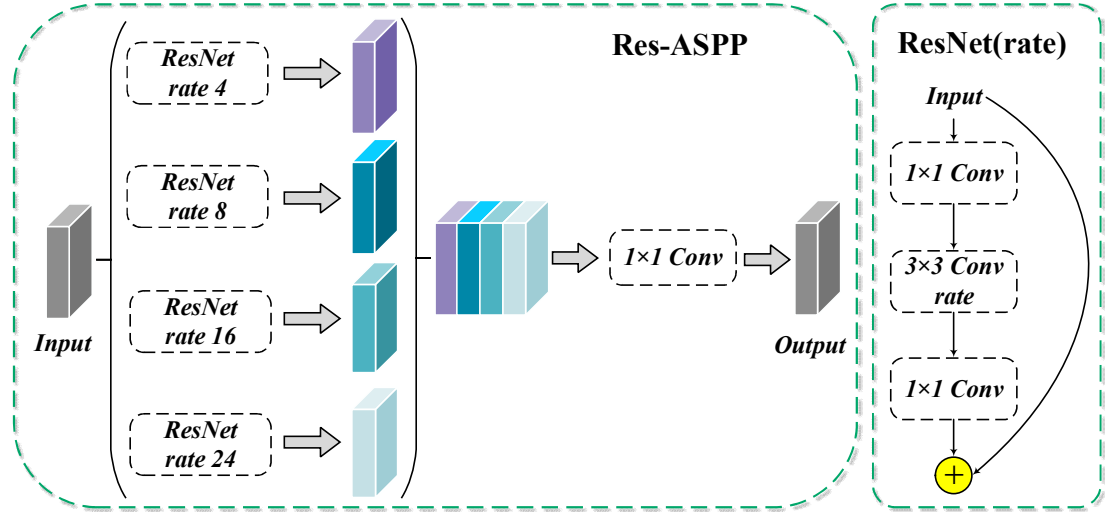


Fig.4. The framework for Res-ASPP, which contains the ResNet module

3.5 Loss function

We use Cross Entropy loss as the loss function for three medical image segmentation datasets to estimate the degree of similarity between the actual and the predicted pictures. The lower the similarity of the pictures, the better the predictions. The specific formula is as follows.

$$L_{seg} = -\sum_{i=1}^N (Y_i \cdot \log(\hat{Y}_p)) \quad (5)$$

Where $Y = \{Y_1, Y_2 \dots Y_t\}$ represents ground truths probabilities, \hat{Y} represents predicted

probabilities, and N represents batch size.

3.6 Evaluation Metrics

To evaluate the segmentation result in ISIC2018, BAA, and COVID-19 CXR datasets, we measured F1 (balanced F Score), MIoU (Mean Intersection over Union). Note that to describe the segmentation metrics better, we introduce a confusion matrix to represent the prediction effect of the classifier on the test datasets. Meanwhile, we take advantage of Params Size (MB) and MACs (G) to measure the parameters and complexity of the model, respectively. N represents the number of pictures. The specifics definition are as follows.

1. FN (False Negative): The predicted negative sample is positive.
2. FP (False Positive): The predicted positive sample is negative.
3. TN (True Negative): Both predictions and facts are negative samples.
4. TP (True Positive): Both predictions and facts are positive samples.

$$F1 = \frac{2TP}{2TP + FP + FN} \quad (6)$$

$$MIoU = \frac{1}{N+1} \sum_{i=0}^N \frac{TP}{TP + FP + FN} \quad (7)$$

4 Experiments

4.1 Datasets

To demonstrate the generalization ability of this network, sufficient experiments were done in ISIC2018, BAA, and COVID-19 CXR datasets.

ISIC 2018. The ISIC 2018 dataset is from the International Skin Imaging Collaborative (ISIC) [22]. In ISIC 2018, task1 was to segment skin lesion tumors under dermoscopy which contains 2594 original images and 2594 manually annotated labels. We resize each picture to 224×224 .

BAA (Bone Age Assessment). The private dataset was obtained from the Affiliated Hospital of Chongqing Medical University, which included 387 original images from X-rays and 387 manually annotated labels. It is used to detect the age and growth of children by hand bone morphology. We selected 310 of the manually annotated images as the training set and the rest of the images as the test set. We resize each picture to 512×512 .

COVID-19 CXR. This dataset was derived from a chest X-ray database containing neo-coronary-positive patients [23-24]. Currently, there are 3616 novel coronaviruses positive, 10,192 normal and 6,012 non new coronaviruses infected CXR images (which have been manually annotated). We selected the novel coronaviruses positive images and their labels for analysis. We used 2892 manually annotated images as the training set and the remaining images as the test set. We resize each picture to 224×224 .

4.2 Implementation details

We use the Pytorch framework to validate the stability of the MS-DC-UNeXt model. We use Adam as an optimizer and Cross Entropy to train our model. The initial learning rate is 0.001 in all three experiments, and the default batch setting of the model is equal to 8 in the ISIC 2018 and COVID-19 datasets and 4 in the BAA dataset. All investigations are done on an RTX-3090 GPU with 30GB of RAM and a 7-core CPU. As the purpose of this experiment is to justify the reasonability of the framework, we did not perform data augmentation on the original images and their labels.

4.3 Experiment results on ISIC 2018 dataset

In the ISIC 2018 dataset, we compare MS-DC-UNeXt with several state-of-the-arts model:1) UNet [3], 2) UNet++ [4], 3) Attention U-Net [6]. We also compare several recent baselines:1) TransUNet [11], 2) Swin-UNet [12], 3) DCSAU-Net [21], 4) UNeXt [16]. Note that we utilized MIoU and F1 to measure the quality of the segmentation and Params Size and MACs to measure the parameters and complexity of the model. We also utilize two-by-two paired t-tests to measure the difference between baselines and MS-DC-UNeXt.

We record the specific experimental results in the Table 1. We can observe that MS-DC-UNeXt achieves the best segmentation results among all the models, and the model performance is significantly improved with similar parameters and complexity as UNeXt. It also achieves good results with its lighter weight structure, which combines accuracy and complexity. We reduce the Params Size by 32 times while decreasing the computational complexity by 47 times. The model prediction performance (MIoU) instead raises by 3.95% when compared with TransUNet. After a two-by-two paired t-test, we can see that all baselines differ from MS-DC-UNeXt on MIoU.

Table 1. Performance Comparison on the ISIC 2018 Dataset(two-by-two paired t-test by comparing the values of MIoU)

Networks	Year	Params Size(MB)	MACs(G)	F1	MIoU	p
UNet	2015	118.40	41.81	86.62	76.66	0.000***
UNet++	2018	39.89	28.68	87.73	78.33	0.001***
Attention U-Net	2018	133.05	101.82	87.51	77.91	0.000***
TransUNet	2021	254.88	24.95	86.59	76.52	0.000***
Swin-UNet	2021	160.08	8.80	86.38	76.17	0.000***
DCSAU-Net	2022	9.89	4.89	88.41	79.39	0.000***
UNeXt	2022	5.61	0.42	87.90	78.56	0.000***
MS-DC-UNeXt	-	7.90	0.53	88.47	79.54	-
MS-DC-UNeXt-S	-	1.36	0.09	87.92	78.62	0.000***

We selected several images of skin cancer lesions with challenging segmentation in ISIC 2018, and the segmentation effects of different models are shown in Figure 5. We also offer the contrast between MIoU, Params Size (MB), and MACs (G) of each baseline in Figure 8(a). The red boxes highlight the regions where MS-DC-UNeXt can do better than the other baselines. It can be seen that TransUNet and Swin-UNet did not show the segmentation advantage in small sample datasets, while UNet and UNet++ did not handle the contextual semantic information correctly, resulting in severe loss of location information. DCSAU-Net can obtain an approximately correct segmentation contour, but it is easily over-segmented and does not correctly understand the information at the edge of the lesion. MS-DC-UNeXt achieves good segmentation results in challenging datasets, and the lesion edges are clearly segmented.

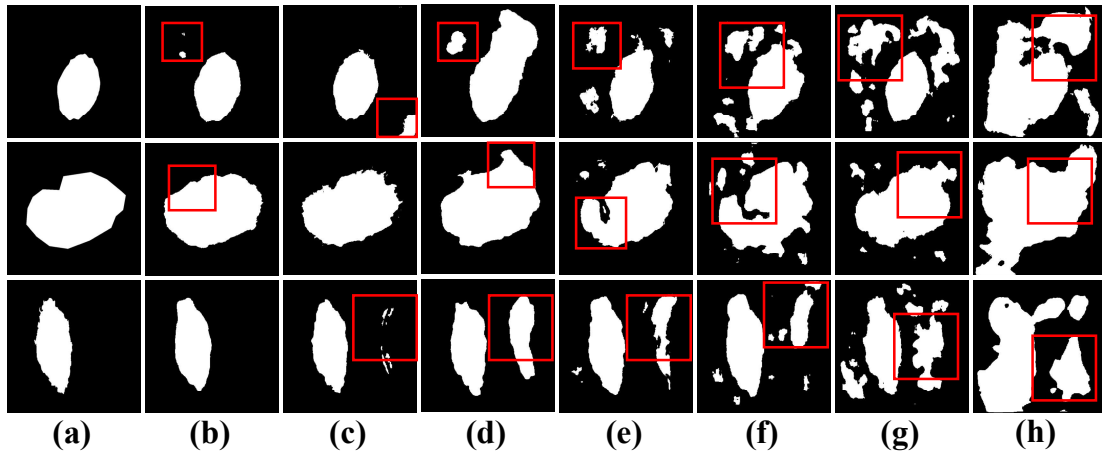


Fig.5. Comparison of segmentation performance of several baseline models on the ISIC 2018 dataset.(a) Ground Truth,(b) MS-DC-UNeXt,(c) DCSAU-Net,(d) MS-DC-UNeXt-S,(e)Attention U-Net,(f)UNet,(g)UNet++,(h)UNeXt.

4.4 Experiment results on BAA dataset

The proposed MS-DC-UNeXt was trained on the BAA dataset to perform hand bone segmentation with a specific experimental procedure similar to the ISIC 2018 dataset. The experimental details are shown in Table 2. We can discover that MS-DC-UNeXt has a remarkable improvement in prediction, with MIoU gains ranging from 0.61% to 3.8%. In particular, a more clear hand-bone boundary can be segmented after applying the Multi-Scale semantic fusion approach to the UNeXt. This is due to the ability of MS-DC-UNeXt will essentially diminish the information loss after downsampling compressed images, which results in more delicate low-level cues. MS-DC-UNeXt also yields good segmentation results with 3.8% and 2.0% improvement in MIoU and F1, compared with the transformer-based model, TransUNet. Finally, even though UNet++ has clear advantages in small datasets, it can not fully trade-off the accuracy and efficiency. It has achieved competitive segmentation results based on huge parameters, which remarkably decrease its efficiency. It is evident that MS-DC-UNeXt has a significant advantage contrasted with the other CNN-based and Transformer-based U-shape models on the BAA dataset.

Table 2. Performance Comparison on the BAA Dataset(two-by-two paired t-test by comparing the values of MIoU)

Networks	Year	Params Size(MB)	MACs(G)	F1	MIoU	p
UNet	2015	118.40	218.44	92.68	86.51	0.000***
UNet++	2018	39.89	149.86	94.01	88.82	0.007***
Attention U-Net	2018	133.05	265.99	92.96	86.90	0.000***
TransUNet	2021	254.83	129.37	92.50	86.13	0.000***
SmaAt-UNet	2021	15.38	77.92	93.45	87.87	0.000***
DCSAU-Net	2022	9.89	25.59	93.89	88.61	0.000***
UNeXt	2022	5.61	2.21	94.01	88.83	0.264
MS-DC-UNeXt	-	7.90	2.73	94.34	89.37	-
MS-DC-UNeXt-S	-	1.36	0.49	93.70	88.22	0.000***

In Figure 6, we visualize the segmentation effect of MS-DC-UNeXt and several baselines under the BAA dataset. We also offer the contrast between MIoU, Params Size (MB), and MACs (G) of each baseline in Figure 8(b). The specific results are shown in Figure 6. Most baselines have over-segmentation and under-segmentation in the small sample dataset because they lose too much important information. It is distinct that MS-DC-UNeXt performs better than the other baselines because it obtains accurate position information so that it has more contiguous segmentation boundaries. The results show that learning Multi-Scale features in MS-DC-UNeXt enhances segmentation accuracy.

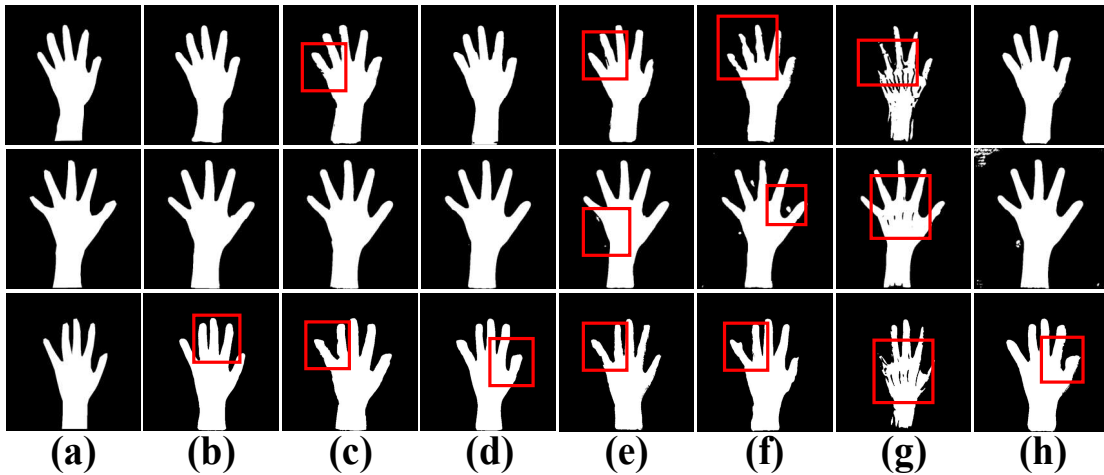


Fig.6. Comparison of segmentation performance of several baseline models on the BAA dataset.(a)Ground Truth,(b)MS-DC-UNeXt,(c)UNet,(d)UNet++,(e)Attention U-Net, (f)MS-DC-UNeXt-S, (g)UNeXt,(h) DCSAU-Net.

4.5 Experiment results on COVID-19 CXR dataset

We trained the MS-DC-UNeXt model on the COVID-19 CXR dataset to perform lung segmentation, and the details of the experimental results are shown in Table 3. The segmentation performance improvement of the MS-DC-UNeXt model on the COVID-19 CXR dataset is not as significant. However, they still have favorable

aspects, with MIoU gains ranging from 0.84% to 2.35%. Note that MS-DC-UNeXt achieves the best segmentation performance considering segmentation accuracy and efficiency, and the parameter size of UNet++ is approximately five times larger than that of MS-DC-UNeXt. Still, the final prediction is not as good as MS-DC-UNeXt. Compared with the lighter UNeXt model, MS-DC-UNeXt has a slight increase in parameter size, but the massive improvement in prediction effect cannot ignore.

Table 3. Performance Comparison on the COVID-19 CXR Dataset(two-by-two paired t-test by comparing the values of MIoU)

Networks	Year	Params Size(MB)	MACs(G)	F1	MIoU	p
UNet++	2018	39.89	28.68	98.57	97.19	0.813
DCSAU-Net	2022	9.89	4.89	98.53	97.12	0.512
UNeXt	2022	5.61	0.42	98.17	96.42	0.001***
MS-DC-UNeXt	-	7.90	0.53	98.99	98.01	-
MS-DC-UNeXt-S	-	1.36	0.09	97.83	95.76	0.000***

We present a few challenging two-lung segmentation results, which are evaluated by labeling False Positive and False Negative regions, as shown in Figure 7. Simultaneously, we also offer the contrast between MIoU, Params Size (MB), and MACs (G) of each baseline in Figure 8(c). We find that MS-DC-UNeXt and its lightweight network achieve the best segmentation results, with relatively few False Positive and False Negative regions due to their ability to take into account high-level and low-level features. DCSAU-Net and UNeXt can segment the contours of both lungs with relatively few false-negative areas, but there are a large number of over-segmented (False Positive) regions. While UNet++ could integrate features between different levels, understanding advanced features in the actual segmentation process was slightly poor, resulting in some unsegmented (False Negative) regions. At the same time, it can also prove that MS-DC-UNeXt and its lightweight network have significant advantages in X-ray image segmentation.

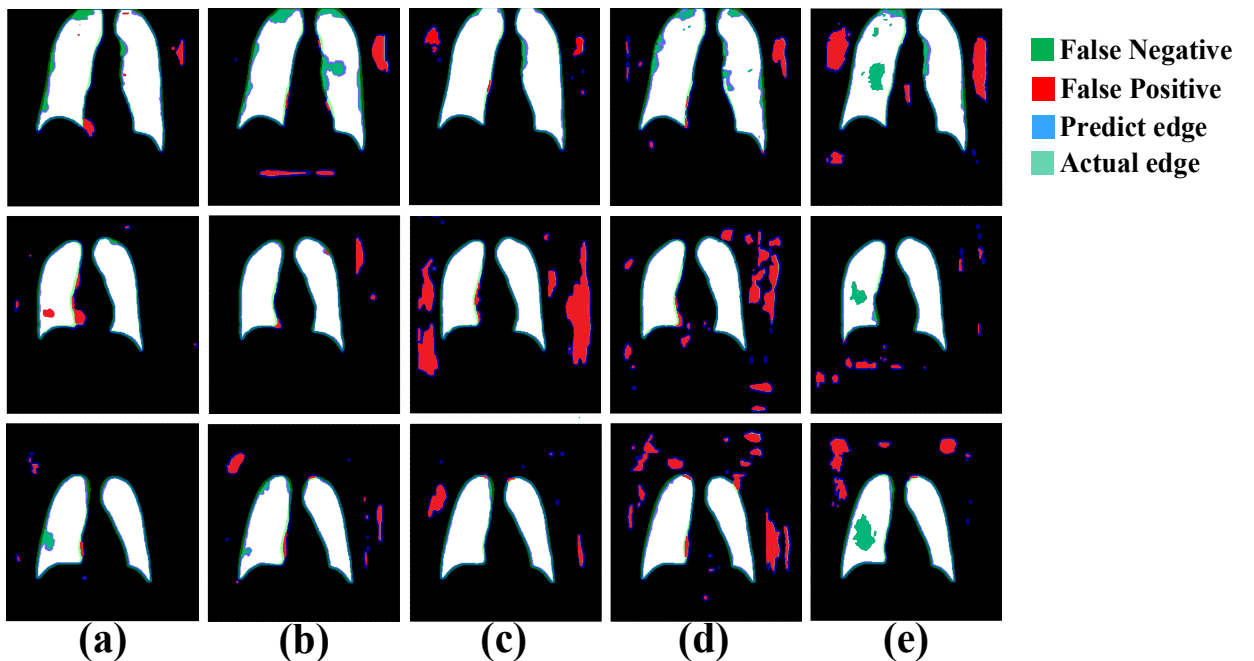


Fig.7. A few segmented images with blurred edges and a high number of false-positive and false-negative regions are selected from the prediction results of the baseline model. (a) MS-DC-UNeXt, (b) MS-DC-UNeXt-S, (c) DCSAU-Net, (d) UNeXt, (e) UNet++.

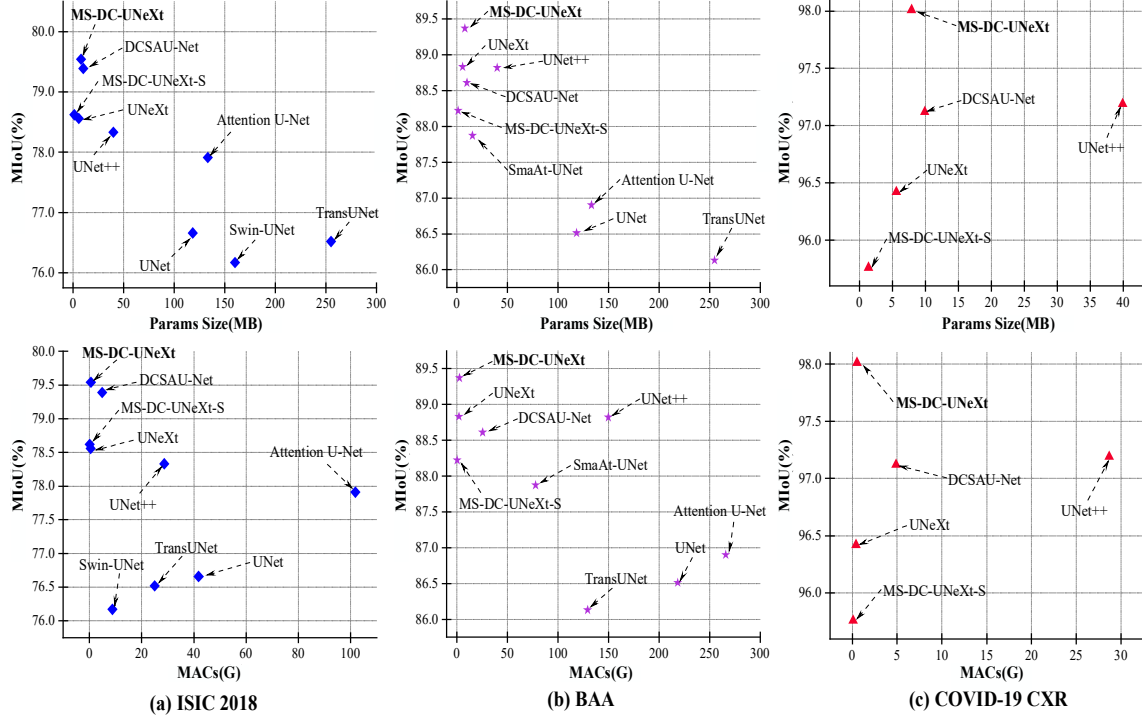


Fig.8. The prediction results of each baseline model are compared on different datasets. Y-axis represents MIoU, where larger values represent better model accuracy. X-axis represents Params Size (MB) and MACs (G), where smaller values represent higher model prediction efficiency. Combining the results of the three datasets, we found that MS-DC-UNeXt can better trade-off the relationship between efficiency and accuracy than the lightweight UNeXt model and ultimately achieve better prediction results.

4.6 Ablation Study

To evaluate the effect of each module on the structure, we performed detailed ablation study, including: 1) the target module, 2) the effect of dilation rate on Res-ASPP, 3) the different numbers of Tok-MLP block, and 4) the number of channels.

The Impact of the target module

Each module plays a different role in the model, and we did more than stack the modules on top of each other randomly. We can see the specific results in Table 4. Firstly, we start with the baseline model(UNet), which shows performance improvements after introducing the tokenized MLP block. To reduce semantic differences, we changed the bottom layer of the tokenized MLP block to Res-ASPP. We changed the single-layer convolution block to the DC-block to obtain more contextual information. We tried to merge the two blocks and got a positive answer.

Note that we have a significant performance improvement with a slight increase in parameters and complexity. Finally, we introduce the Attention Gate module in the decoder to focus on the valuable information. Compared with the initial model version, we decreased a considerable number of parameters and complexity to obtain a more robust model.

Table 4. Ablation Study on the target module

Networks	Params Size(MB)	MACs(G)	F1	MIoU
Baseline(Unet)	118.40	41.81	86.62	76.66
Baseline+Tok-MLP	5.61	0.42	87.90	78.56
Baseline+Tok-MLP+Res-ASPP	6.30	0.54	88.11	79.01
Baseline+Tok-MLP+DC-Conv	5.49	0.42	88.12	79.05
Baseline+Tok-MLP+DC-Conv+Res-ASPP	7.74	0.49	88.27	79.25
Baseline+Tok-MLP+DC-Conv+Res-ASPP+AG	7.90	0.53	88.47	79.54

The effect of dilation rate on Res-ASPP

Dilated Convolution obtains a Multi-Scale receptive field by shifting the number of kernel spacings to capture more contextual semantic information. The following Table 5 compares the effects of choosing different dilation rates on the model when all other conditions are the same. With dilation rates of 4,8,16,24, the network achieves more remarkable performance with 0.3% and 0.6% improvement in F1 and MIoU, respectively.

Table 5. Ablation Study on the effect of dilation rate

r1	r2	r3	r4	F1	MIoU
2	4	8	12	87.98	78.72
4	8	16	24	88.11	79.01
6	12	18	24	87.86	78.53

Discuss on different numbers of Tok-MLP block

As mentioned above, Tokenized MLP block helps mark segmentation details, feature projection and reduces model parameters and complexity. This part of the ablation study will specifically discuss the effect of different numbers of the Tok-MLP block on the prediction effect. We can see the specific results in Table 6. Note that when we set the Tok-MLP block on the third and fourth layers, we can obtain finer segmentation details with a slight increase in parameters. Based on the previous basis, we set the Tok-MLP block at the second layer, and the segmentation performance increases insignificantly with a slight rise in parameters. We finally decided to put the Tok-MLP block in the third and fourth layers, and F1 and MIoU improved by 1.2% and 2.1%, respectively.

Table 6. Ablation Study on different positions of Tok-MLP

Baseline(Unet)	Res-ASPP	Tok-MLP			Params Size(MB)	F1	MIoU
		(4)	(3)	(2)			
✓	✓	✓			6.17	87.04	77.38
✓	✓	✓	✓		6.30	88.11	79.01
✓	✓	✓	✓	✓	6.44	88.09	78.87

Analysis on number of channels

Appropriately increasing the number of channels can improve the performance of the network. The following Table 7 compares the segmentation performance of small, medium, and extensive networks, respectively. Although the small network (MS-DC-UNeXt-S) is extremely lightweight, the commission cannot be regarded as perfect. After increasing the network channels (MS-DC-UNeXt-L), the performance has a slight push but causes a colossal computing cost. We finally chose the medium-sized network (MS-DC-UNeXt-M), which can better trade off the accuracy and segmentation speed.

Table 7. Ablation Study on number of channels

Networks	C1	C2	C3	C4	C5	Params Size(MB)	MACs(G)	F1	MIoU
MS-DC-UNeXt-S	8	16	32	64	128	1.36	0.09	87.91	78.58
MS-DC-UNeXt-M	16	32	128	160	256	7.90	0.53	88.47	79.54
MS-DC-UNeXt-L	32	64	128	256	512	21.47	1.47	88.58	79.69

5 Conclusion

In this paper, we analyze the advantages and disadvantages of classical CNN-based and Transformer-based models and find the shortcomings of UNeXt models, which are improved on this original basis. We discovered that UNeXt is too lightweight, leading to blurred segmentation boundaries due to excessive semantic gaps in the actual prediction process. We have designed a symmetric Encoder-Decoder MS-DC-UNeXt model, leveraging DC-block and Res-ASPP block to obtain Multi-Scale features. Two linear layers are used to get a self-attention mechanism similar to the transformer, which makes the MS-DC-UNeXt model semantic dependency of local-to-global. We have improved and enlarged the scope of use of the original UNeXt model, and the segmentation effect is significantly enhanced with a slight amount of additional parameters and operational complexity. We performed full validation on a benchmark dataset (ISIC 2018) and two X-ray image datasets to measure the prediction performance of the MS-DC-UNeXt model. All three datasets contain challenging images, which we predict by selecting X-ray images with low contrast, a large number of Artifacts, and ill-defined boundaries. MS-DC-UNeXt can outperform the other U-shape networks on these challenging images. Other baselines have blurred segmentation margins and even completely miss segmentation objects during the prediction process. Note that TransUNet has 32 times more parameters than MS-DC-UNeXt, while MS-DC-UNeXt has significantly better prediction performance than TransUNet. Thus, we can judge that MS-DC-UNeXt has extremely high generalization ability and robustness, and it can become a powerful helper to help doctors deal with X-ray images. Dedicated to optimizing the network structure, in the future, we will continue to refine the MS-DC-UNeXt model. We will generalize its applicability from X-ray to CT and MRI datasets [25] and look for universal segmentation methods.

References

- [1] Asgari Taghanaki S, Abhishek K, Cohen J P, et al. Deep semantic segmentation of natural and medical images: a review[J]. *Artificial Intelligence Review*, 2021, 54(1): 137-178.
- [2] Long J, Shelhamer E, Darrell T. Fully convolutional networks for semantic segmentation[C]//*Proceedings of the IEEE conference on computer vision and pattern recognition*. 2015: 3431-3440.
- [3] Ronneberger O, Fischer P, Brox T. U-net: Convolutional networks for biomedical image segmentation[C]//*International Conference on Medical image computing and computer-assisted intervention*. Springer, Cham, 2015: 234-241.
- [4] Zhou Z, Rahman Siddiquee M M, Tajbakhsh N, et al. Unet++: A nested u-net architecture for medical image segmentation[M]//*Deep learning in medical image analysis and multimodal learning for clinical decision support*. Springer, Cham, 2018: 3-11.
- [5] Huang H, Lin L, Tong R, et al. Unet 3+: A full-scale connected unet for medical image segmentation[C]//*ICASSP 2020-2020 IEEE International Conference on Acoustics, Speech and Signal Processing (ICASSP)*. IEEE, 2020: 1055-1059.
- [6] Oktay O, Schlemper J, Folgoc L L, et al. Attention u-net: Learning where to look for the pancreas[J]. *arXiv preprint arXiv:1804.03999*, 2018.
- [7] Jha D, Smedsrud P H, Riegler M A, et al. Resunet++: An advanced architecture for medical image segmentation[C]//*2019 IEEE International Symposium on Multimedia (ISM)*. IEEE, 2019: 225-2255.
- [8] Lou A, Guan S, Loew M. DC-UNet: rethinking the U-Net architecture with dual channel efficient CNN for medical image segmentation[C]//*Medical Imaging 2021: Image Processing*. SPIE, 2021, 11596: 758-768.
- [9] Dosovitskiy A, Beyer L, Kolesnikov A, et al. An image is worth 16x16 words: Transformers for image recognition at scale[J]. *arXiv preprint arXiv:2010.11929*, 2020.
- [10] Liu Z, Lin Y, Cao Y, et al. Swin transformer: Hierarchical vision transformer using shifted windows[C]//*Proceedings of the IEEE/CVF International Conference on Computer Vision*. 2021: 10012-10022.
- [11] Chen J, Lu Y, Yu Q, et al. Transunet: Transformers make strong encoders for medical image segmentation[J]. *arXiv preprint arXiv:2102.04306*, 2021.
- [12] Cao H, Wang Y, Chen J, et al. Swin-unet: Unet-like pure transformer for medical image segmentation[J]. *arXiv preprint arXiv:2105.05537*, 2021.
- [13] Fan C M, Liu T J, Liu K H. SUNet: Swin Transformer UNet for Image Denoising[J]. *arXiv preprint arXiv:2202.14009*, 2022.
- [14] Tolstikhin I O, Houlsby N, Kolesnikov A, et al. Mlp-mixer: An all-mlp architecture for vision[J]. *Advances in Neural Information Processing Systems*, 2021,

34: 24261-24272.

[15]Lian D, Yu Z, Sun X, et al. As-mlp: An axial shifted mlp architecture for vision[J]. arXiv preprint arXiv:2107.08391, 2021.

[16]Valanarasu J M J, Patel V M. UNeXt: MLP-based Rapid Medical Image Segmentation Network[J]. arXiv preprint arXiv:2203.04967, 2022.

[17]Masood S, Sharif M, Masood A, et al. A survey on medical image segmentation[J]. Current Medical Imaging, 2015, 11(1): 3-14.

[18]Minaee S, Boykov Y Y, Porikli F, et al. Image segmentation using deep learning: A survey[J]. IEEE transactions on pattern analysis and machine intelligence, 2021.

[19]LeCun Y, Bottou L, Bengio Y, et al. Gradient-based learning applied to document recognition[J]. Proceedings of the IEEE, 1998, 86(11): 2278-2324.

[20]Trebing K, Stańczyk T, Mehrkanoon S. SmaAt-UNet: Precipitation nowcasting using a small attention-UNet architecture[J]. Pattern Recognition Letters, 2021, 145: 178-186.

[21]Xu Q, Duan W, He N. DCSAU-Net: A Deeper and More Compact Split-Attention U-Net for Medical Image Segmentation[J]. arXiv preprint arXiv:2202.00972, 2022.

[22]Codella N C F, Gutman D, Celebi M E, et al. Skin lesion analysis toward melanoma detection: A challenge at the 2017 international symposium on biomedical imaging (isbi), hosted by the international skin imaging collaboration (isic)[C]//2018 IEEE 15th international symposium on biomedical imaging (ISBI 2018). IEEE, 2018: 168-172.

[23]Chowdhury M E H, Rahman T, Khandakar A, et al. Can AI help in screening viral and COVID-19 pneumonia?[J]. IEEE Access, 2020, 8: 132665-132676.

[24]Rahman T, Khandakar A, Qiblawey Y, et al. Exploring the effect of image enhancement techniques on COVID-19 detection using chest X-ray images[J]. Computers in biology and medicine, 2021, 132: 104319.

[25]Wahlund L O, Barkhof F, Fazekas F, et al. A new rating scale for age-related white matter changes applicable to MRI and CT[J]. Stroke, 2001, 32(6): 1318-1322.